Enhanced thermal stability of silica-coated gold nanorods for photoacoustic imaging and image-guided therapy

Yun-Sheng Chen,[1,2] Wolfgang Frey,[1] Seungsoo Kim,[1] Kimberly Homan,[1] Pieter Kruizinga,[1] Konstantin Sokolov,[1,3] and Stanislav Emelianov[1,2,3*]

[1]*Department of Biomedical Engineering, University of Texas at Austin, Austin, TX, 78712, USA*
[2]*Department of Electrical and Computer Engineering, University of Texas at Austin, Austin, TX, 78712, USA*
[3]*Department of Imaging Physics, University of Texas M.D. Anderson Cancer Center, Houston, Texas 77030, USA*
**emelian@mail.utexas.edu*

Abstract: Photothermal stability and, therefore, consistency of both optical absorption and photoacoustic response of the plasmonic nanoabsorbers is critical for successful photoacoustic image-guided photothermal therapy. In this study, silica-coated gold nanorods were developed as a multifunctional molecular imaging and therapeutic agent suitable for image-guided photothermal therapy. The optical properties and photothermal stability of silica-coated gold nanorods under intense irradiation with nanosecond laser pulses were investigated by UV-Vis spectroscopy and transmission electron microscopy. Silica-coated gold nanorods showed increased photothermal stability and retained their superior optical properties under much higher fluences. The changes in photoacoustic response of PEGylated and silica-coated nanorods under laser pulses of various fluences were compared. The silica-coated gold nanorods provide a stable photoacoustic signal, which implies better imaging capabilities and make silica-coated gold nanorods a promising imaging and therapeutic nano-agent for photoacoustic imaging and image-guided photothermal therapy.

OCIS codes: (170.5120) Photoacoustic imaging; (170.3880) Medical and biological imaging

References and links

1. J. Yguerabide, and E. E. Yguerabide, "Light-scattering submicroscopic particles as highly fluorescent analogs and their use as tracer labels in clinical and biological applications," Anal. Biochem. **262**(2), 157–176 (1998).
2. S. Kumar, N. Harrison, R. Richards-Kortum, and K. Sokolov, "Plasmonic nanosensors for imaging intracellular biomarkers in live cells," Nano Lett. **7**(5), 1338–1343 (2007).
3. J. Aaron, K. Travis, N. Harrison, and K. Sokolov, "Dynamic imaging of molecular assemblies in live cells based on nanoparticle plasmon resonance coupling," Nano Lett. **9**(10), 3612–3618 (2009).
4. S. S. Chang, C. W. Shih, C. D. Chen, W. C. Lai, and C. R. C. Wang, "The shape transition of gold nanorods," Langmuir **15**(3), 701–709 (1999).
5. K. S. Lee, and M. A. El-Sayed, "Gold and silver nanoparticles in sensing and imaging: sensitivity of plasmon response to size, shape, and metal composition," J. Phys. Chem. B **110**(39), 19220–19225 (2006).
6. S. Kumar, J. Aaron, and K. Sokolov, "Directional conjugation of antibodies to nanoparticles for synthesis of multiplexed optical contrast agents with both delivery and targeting moieties," Nat. Protoc. **3**(2), 314–320 (2008).
7. S. Mallidi, T. Larson, J. Aaron, K. Sokolov, and S. Emelianov, "Molecular specific optoacoustic imaging with plasmonic nanoparticles," Opt. Express **15**(11), 6583–6588 (2007).
8. P. C. Li, C. R. C. Wang, D. B. Shieh, C. W. Wei, C. K. Liao, C. Poe, S. Jhan, A. A. Ding, and Y. N. Wu, "In vivo photoacoustic molecular imaging with simultaneous multiple selective targeting using antibody-conjugated gold nanorods," Opt. Express **16**(23), 18605–18615 (2008).
9. S. Mallidi, T. Larson, J. Tam, P. P. Joshi, A. Karpiouk, K. Sokolov, and S. Emelianov, "Multiwavelength photoacoustic imaging and plasmon resonance coupling of gold nanoparticles for selective detection of cancer," Nano Lett. **9**(8), 2825–2831 (2009).

#124424 - $15.00 USD Received 18 Feb 2010; revised 29 Mar 2010; accepted 30 Mar 2010; published 13 Apr 2010

10. J. Shah, S. Park, S. Aglyamov, T. Larson, L. Ma, K. Sokolov, K. Johnston, T. Milner, and S. Y. Emelianov, "Photoacoustic imaging and temperature measurement for photothermal cancer therapy," J. Biomed. Opt. **13**(3), 034024 (2008).
11. S. Sethuraman, S. R. Aglyamov, R. W. Smalling, and S. Y. Emelianov, "Remote temperature estimation in intravascular photoacoustic imaging," Ultrasound Med. Biol. **34**(2), 299–308 (2008).
12. J. Shah, S. R. Aglyamov, K. Sokolov, T. E. Milner, and S. Y. Emelianov, "Ultrasound imaging to monitor photothermal therapy - feasibility study," Opt. Express **16**(6), 3776–3785 (2008).
13. J. L. West, and N. J. Halas, "Engineered nanomaterials for biophotonics applications: improving sensing, imaging, and therapeutics," Annu. Rev. Biomed. Eng. **5**(1), 285–292 (2003).
14. K. L. Kelly, E. Coronado, L. L. Zhao, and G. C. Schatz, "The optical properties of metal nanoparticles: The influence of size, shape, and dielectric environment," J. Phys. Chem. B **107**(3), 668–677 (2003).
15. P. K. Jain, K. S. Lee, I. H. El-Sayed, and M. A. El-Sayed, "Calculated absorption and scattering properties of gold nanoparticles of different size, shape, and composition: applications in biological imaging and biomedicine," J. Phys. Chem. B **110**(14), 7238–7248 (2006).
16. M. B. Mohamed, K. Z. Ismail, S. Link, and M. A. El-Sayed, "Thermal reshaping of gold nanorods in micelles," J. Phys. Chem. B **102**(47), 9370–9374 (1998).
17. H. Petrova, J. Perez Juste, I. Pastoriza-Santos, G. V. Hartland, L. M. Liz-Marzán, and P. Mulvaney, "On the temperature stability of gold nanorods: comparison between thermal and ultrafast laser-induced heating," Phys. Chem. Chem. Phys. **8**(7), 814–821 (2006).
18. A. Plech, V. Kotaidis, S. Gresillon, C. Dahmen, and G. von Plessen, "Laser-induced heating and melting of gold nanoparticles studied by time-resolved x-ray scattering," Phys. Rev. B **70**(19), 195423 (2004).
19. Y. T. Wang, S. Teitel, and C. Dellago, "Surface-driven bulk reorganization of gold nanorods," Nano Lett. **5**(11), 2174–2178 (2005).
20. Y. Liu, E. Mills, and R. Composto, "Tuning optical properties of gold nanorods in polymer films through thermal reshaping," J. Mater. Chem. **19**(18), 2704–2709 (2009).
21. Y. Khalavka, C. Ohm, L. Sun, F. Banhart, and C. Soennichsen, "Enhanced thermal stability of gold and silver nanorods by thin surface layers," J. Phys. Chem. C **111**(35), 12886–12889 (2007).
22. N. R. Jana, L. Gearheart, and C. J. Murphy, "Seed-mediated growth approach for shape-controlled synthesis of spheroidal and rod-like gold nanoparticles using a surfactant template," Adv. Mater. **13**(18), 1389–1393 (2001).
23. I. Pastoriza-Santos, J. Perez-Juste, and L. M. Liz-Marzan, "Silica-coating and hydrophobation of ctab-stabilized gold nanorods," Chem. Mater. **18**(10), 2465–2467 (2006).
24. A. T. Heitsch, D. K. Smith, R. E. Patel, D. Ress, and B. A. Korgel, "Multifunctional particles: Magnetic nanocrystals and gold nanorods coated with fluorescent dye-doped silica shells," J. Solid State Chem. **181**(7), 1590–1599 (2008).
25. N. Omura, I. Uechi, and S. Yamada, "Comparison of plasmonic sensing between polymer- and silica-coated gold nanorods," Anal. Sci. **25**(2), 255–259 (2009).
26. I. Gorelikov, and N. Matsuura, "Single-step coating of mesoporous silica on cetyltrimethyl ammonium bromide-capped nanoparticles," Nano Lett. **8**(1), 369–373 (2008).
27. Y.-S. Chen, P. P. Kruizinga, P. Joshia, S. Kim, K. Homan, K. Sokolov, W. Frey, and S. Emelianov, "On stability of molecular therapeutic agents for noninvasive photoacoustic and ultrasound image-guided photothermal therapy," Proc. SPIE **7564**, 7564–7561 (2010).
28. B. Nikoobakht, and M. A. El-Sayed, "Preparation and growth mechanism of gold nanorods (nrs) using seed-mediated growth method," Chem. Mater. **15**(10), 1957–1962 (2003).
29. W. Stober, A. Fink, and E. Bohn, "Controlled growth of monodisperse silica spheres in micron size range," J. Colloid Interface Sci. **26**(1), 62–69 (1968).
30. Y. Lu, Y. D. Yin, B. T. Mayers, and Y. N. Xia, "Modifying the surface properties of superparamagnetic iron oxide nanoparticles through a sol-gel approach," Nano Lett. **2**(3), 183–186 (2002).
31. P. B. Johnson, and R. W. Christy, "Optical constants of the noble metals," Phys. Rev. B **6**(12), 4370–4379 (1972).
32. L. Qiu, T. A. Larson, D. K. Smith, E. Vitkin, S. H. Zhang, M. D. Modell, I. Itzkan, E. B. Hanlon, B. A. Korgel, K. V. Sokolov, and L. T. Perelman, "Single gold nanorod detection using confocal light absorption and scattering spectroscopy," IEEE J. Sel. Top. Quant. **13**(6), 1730–1738 (2007).
33. M. B. Mohamed, T. S. Ahmadi, S. Link, M. Braun, and M. A. El-Sayed, "Hot electron and phonon dynamics of gold nanoparticles embedded in a gel matrix," Chem. Phys. Lett. **343**(1-2), 55–63 (2001).
34. M. Hu, X. Wang, G. V. Hartland, V. Salgueirino-Maceira, and L. M. Liz-Marzan, "Heat dissipation in gold-silica core-shell nanoparticles," Chem. Phys. Lett. **372**(5-6), 767–772 (2003).

1. Introduction

Metal nanoparticles (MNPs) have become highly versatile contrast agents for optical imaging of cells in-vitro and of biological tissue. While it has been known that the quantum yield from spherical gold or silver nanoparticles is orders of magnitude higher than that of organic dyes [1], these spherical particles have recently also been used to study dynamic interactions and receptor clustering in cells using their sensitivity to the proximity of other MNPs and the

#124424 - $15.00 USD Received 18 Feb 2010; revised 29 Mar 2010; accepted 30 Mar 2010; published 13 Apr 2010

plasmonic resonance coupling [2,3]. The formation of MNPs into other shapes, such as rods, shells, cubes, triangles, bipyramids, etc., has allowed for a relatively free choice of the wavelength, including the "transparent" range of wavelengths in the near infra-red (NIR) range where tissues absorb minimally [4,5]. The large surface area and simple chemistry of the nanoparticles makes it easy to develop complex recognition and targeting strategies for molecular imaging and site specific therapy [6]. In addition, new imaging and therapeutic techniques, such as photoacoustic molecular imaging and photothermal therapy, have been developed where unique properties of these particles are used to achieve enhanced contrast between MNPs and tissue [7–9].

Among these new developing techniques, molecular specific photoacoustic and ultrasound image-guided photothermal therapy was proposed to treat various medical conditions, such as cancer [10–12]. Photothermal therapy relies on the resonant absorption of light by the nanoparticle and the conversion of the electromagnetic energy into heat to destroy malignant tissue [10–13]. At the same time, nanoparticle-facilitated absorption of pulsed light leads to the production of sound waves used for photoacoustic imaging. In image-guided photothermal therapy, photoacoustic imaging can be used both to confirm the delivery of MNPs to the desired location in tissue and to visualize temperature maps during photothermal therapy [10]. The absolute as well as relative strength of the surface plasmon resonant absorption and scattering that contribute to the well defined extinction band of gold or silver MNPs depend on the nanoparticle material composition, shape, and environment [14]. While large scattering cross sections are needed for dark-field imaging, large absorption cross sections are required for photoacoustic imaging [15]. Therefore nanospheres, nanoshells, nanocages, nanoplates and nanorods are used in photoacoustic imaging. Gold nanorods are particularly interesting as they are small, easy to synthesize, have a tunable resonance in the red and NIR spectrum, and possess a very high absorption cross section.

During photoacoustic imaging gold nanorods are exposed to high-energy nanosecond laser pulses. The nanorods absorb a portion of the light and generate substantial heat that can lead to nanorod reshaping and an associated reduction in absorption cross section. Nanoparticle melting has been shown for nanospheres and nanorods to occur at significantly lower temperatures than bulk melting of the metal, in part because surface reorganization processes dominate [4, 16–18]. Results of numerical simulations indicate that for thin nanorods, the surface melting can extend into the interior [19]. Nanorods held at fixed temperatures can already melt and form spheres below 100–250 °C depending on the surface coating and the environment in which they are embedded [17, 20]. Several studies have shown that embedding the nanorods in a solid environment, such as carbon or PMMA, significantly increases photothermal stability; in the latter case below the glass transition temperature only [20, 21].

For the purpose of photothermal therapy guided by molecular photoacoustic imaging and ultrasound, it is highly desirable to have plasmonic nanoabsorbers with a more photothermally stable coating, which also is chemically easy to modify. Silica coating of nanorods has been shown based on several strategies [22–26], and silica can easily be used for bioconjugation [6, 27]. We recently presented preliminary results of the photothermal stability of silica-coated gold nanorods [27], and here we provide a detailed study of the stability of silica-coated gold nanorods of different shell thickness under nanosecond laser pulse illumination at 800 nm, and compare the results to the photothermal stability of cetyltrimethyl-ammoniumbromide (CTAB) stabilized gold nanorods and poly ethylene glycol (PEG) coated gold nanorods.

2. Methods

2.1 Synthesis of silica-coated gold nanorods

All chemicals used in this study were used as received: cetyltrimethyl-ammoniumbromide (CTAB, Sigma), gold(III) chloride hydrate ($HAuCl_{4(aq)}$, Aldrich), sodium borohydride

#124424 - $15.00 USD Received 18 Feb 2010; revised 29 Mar 2010; accepted 30 Mar 2010; published 13 Apr 2010

($NaBH_4$, Sigma), silver nitrate ($AgNO_3$, Sigma), O-(2-mercaptoethyl)-O'-methyl-hexa(ethylene glycol) (mPEG-thiol, MW. 5,000, Laysan Bio), ammonia (Fisher Scientific), 2-propanol (Fisher Scientific), and tetraethyl orthosilicate (TEOS, Aldrich).

Silica-coated gold nanorods were produced from CTAB-stabilized gold nanorods by exchanging CTAB with the biocompatible mPEG-thiol, and then using the mPEG polymer as a silane coupling agent for silica coating [27]. In the first step, CTAB stabilized gold nanorods were synthesized by seed-mediated growth following Jana *et al.* [22] and Nikoobakht *et al.* [28]: 5 mL of $CTAB_{(aq)}$ solution (0.20 M) was first mixed with 5 mL of $HAuCl_{4(aq)}$ solution (0.5 mM). Then, 0.60 mL of ice-cold $NaBH_{4(aq)}$ solution (0.01 M) was added to the mixture and vigorously stirred for 2 min at 25°C, which resulted in the formation of a brownish yellow seed solution. The growth solution was made by adding 0.15–0.2 mL $AgNO_{3(aq)}$ (4 mM) and then 5 mL of $HAuCl_{4(aq)}$ (1 mM) solutions to 5 mL of $CTAB_{(aq)}$ (0.20 M) solution, under gentle mixing, followed by 70 μL of ascorbic acid (0.0788 M) solution. To grow nanorods, 12 μL of the seed solution was added to the growth solution at 27–30 °C under gentle stirring for 30 seconds. The transparency of the solution changed to burgundy red within 10–20 min. The solution then aged for another 12 hours at 27–30 °C, before being centrifuged at 18,000 g for 45 min, twice. The collected nanorods were re-dispersed in ultrafiltrated (18 MΩcm, Thermo Scientific Barnstead Diamond water purification systems) deionized water. In the second step, the stabilization agent, CTAB, on the surface of the gold nanorods was replaced by mPEG-thiol through ligand exchange. Briefly, the CTAB-stabilized gold nanorod dispersion was added to an equal volume of mPEG-thiol (0.2 mM) aqueous solution under vigorous stirring. The mixture was sonicated for 5 minutes and left to react for 2 hours. Excess mPEG-thiol molecules were removed by centrifugation filtration (Amicon ultra-15, Millipore) at 3000 g for 10 min and the PEGylated gold nanorods were re-suspended in water. In the last step, a modified Stöber method [29, 30] was used to grow a silica shell of controlled thickness on the PEGylated gold nanorods. The PEGylated gold nanorod suspension (1.2 mL) was added under vigorous stirring to 1.8 mL of isopropanol, then an ammonia solution in isopropanol (3.84 vol.% ammonia (33 wt%)) was added slowly under vigorous stirring until the solution reached pH = 11. Finally, 0.04 mL-0.40 mL of a solution of TEOS in isopropanol (100 mM) was added under gentle stirring, depending on the desired shell thickness. The reaction mixture was allowed to react for 2 hours. The above procedure produces silica shells with an adjustable thickness from 6 nm to 20 nm.

2.2 Characterization of the photothermal stability of the nanorods

Nanorod stability under nanosecond pulsed laser exposure was optically characterized by ultraviolet to visible (UV-Vis) extinction spectroscopy. Extinction spectra were collected from a 50 μL nanorod suspension in a 96-well microliter plate reader (BioTek Synergy HT) at room temperature before and after laser exposure. An 800 nm wavelength laser beam, generated by a tunable OPO laser system (Vibrant, OPOTEK, Inc.), was collimated to fully illuminate each well from the top. Three hundred pulses of 7 ns pulse duration at 10 Hz repetition rate were applied with average fluence from 4 ± 0.13 mJ/cm^2 to 20 ± 0.65 mJ/cm^2. The average fluence and its standard deviation were calculated by recording the fluence of the 300 pulses using a calibrated beam splitter.

The shape and morphology changes of the gold nanorods were monitored by transmission electron microscopy (TEM) imaging. For TEM imaging, a drop of gold nanorod suspension was placed on copper-Formvar grids and blotted dry with a filter paper. The grids were imaged using the TEM mode of a Hitachi S-5500 FESEM equipped with a field emission electron source operated at 30 kV.

A custom-made ultrasound and photoacoustic imaging system (Fig. 1(a)) was used to test the photothermal stability of nanorods by measuring the photoacoustic signal from aqueous solutions of either PEG-coated or silica-coated nanorods. A 1mm diameter glass tube was fixed in an acrylate water tank containing an optical window inlay. The glass tube contains an

#124424 - $15.00 USD Received 18 Feb 2010; revised 29 Mar 2010; accepted 30 Mar 2010; published 13 Apr 2010

inlet and an outlet for injecting the samples into the glass tube without moving the tube during the experiment. Fifty μL of either a PEG-coated gold nanorod or a 20 nm silica-coated gold nanorod solution, each with optical density (O.D.) of 0.5 were injected into the tube through the outlet. A single element focused ultrasound transducer (Panametrics Inc., V320) with 7.5 MHz center frequency, 50.4 mm focal distance, and 13 mm aperture was mounted on a one dimensional positioning stage (Fig. 1(b)). The position of the transducer was adjusted so that the nanorod solution section was located in the center of the ultrasound beam, and the distance between transducer and glass tube was kept constant during the entire experiment. Nanosecond laser pulses were introduced through the optical window into the water tank and uniformly irradiated the sample. For each laser pulse, the photoacoustic signal was captured and stored for off-line processing to estimate the change in photoacoustic signal due to possible photothermal damage to the nanorods. The amplitude of the recorded photoacoustic signal from each pulse was first compensated by the fluence fluctuation factor (calculated from recorded power meter readings per pulse), then the photoacoustic signal of each pulse was normalized to the maximum photoacoustic signal recorded. Three independent measurements have been performed in this study. The average and the standard deviation of the normalized amplitudes of each point are calculated from these three measurements. The averaged normalized amplitudes and their standard deviations were plotted versus pulse number for comparing the photoacoustic signal stability of PEG coated gold nanorods and 20 nm silica-coated gold nanorods.

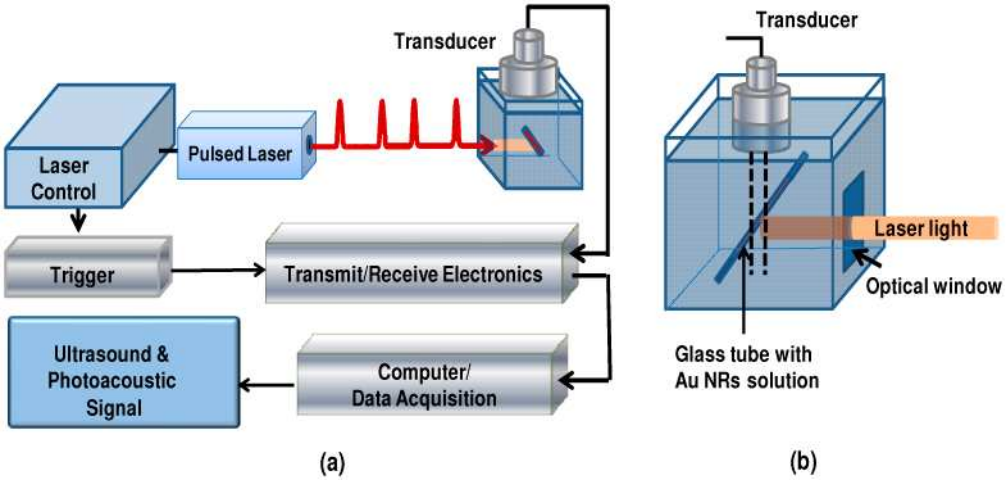

Fig. 1. (a) A block diagram of the ultrasound and photoacoustic imaging system used to evaluate the thermal stability of CTAB-coated, PEG-coated and silica-coated nanorods. (b) Close-up schematic illustration of the sample irradiated by a pulsed laser beam while photoacoustic transients were measured using the ultrasound transducer.

240 nm (> 2 nm). The simulation volume is enclosed by perfectly matched layer (PML) absorbing boundaries. A total-field/scattered-field (TF/SF) source with a spectral pulse from 400 – 1000 nm and a center frequency of 524.6 THz was used to avoid diffraction artifacts from a finite source, and to have a more accurate scattered field. Gold dielectric data was based on Johnson and Christy [31] and the silica refractive index used was 1.459. The ambient was water with a refractive index of 1.33. CTAB and PEG layers were ignored, because their refractive index would depend on the surface coverage, and these layers would lead to less than 10 nm peak shifts to the red. The spectral dependence of the absorption and scattering cross sections for both polarizations were calculated, corrected for random light polarization and nanorod orientation, and added. Nanorods of a total length of 34 nm were modeled as cylinders (25 nm length and 9 nm diameter) with semi-spherical caps of constant

#124424 - $15.00 USD Received 18 Feb 2010; revised 29 Mar 2010; accepted 30 Mar 2010; published 13 Apr 2010

radius of 4.5 nm. For the shortened nanorods in a silica shell the gaps were filled with ambient water. Ellipsoids were calculated to have circular cross section and the same volume as the original gold nanorod, but with progressively shortened long axis, given in percent of the original nanorod length.

3. Results and discussion

A typical UV-Vis extinction spectrum and a corresponding TEM image of gold nanorods with 10 nm of silica shell are shown in Fig. 2. The nanorods are uniformly coated with silica: the thickness is 10.3 ± 1.1 nm. As expected, the UV-Vis spectrum has two extinction bands at 530 nm (transversal; polarization perpendicular to the long axis) and at ~780 nm (longitudinal; polarization along the long axis). While the transversal peak does not shift significantly from bare PEG-coated to silica-coated nanorods, the longitudinal resonance shifts by ~20 nm (Fig. 2(a)). A FDTD simulation of the gold nanorods before and after silica coating is also shown in Fig. 2(a). The experimental spectra are significantly broader than the simulation for a single aspect ratio, which is typical due to some inhomogeneity of the aspect

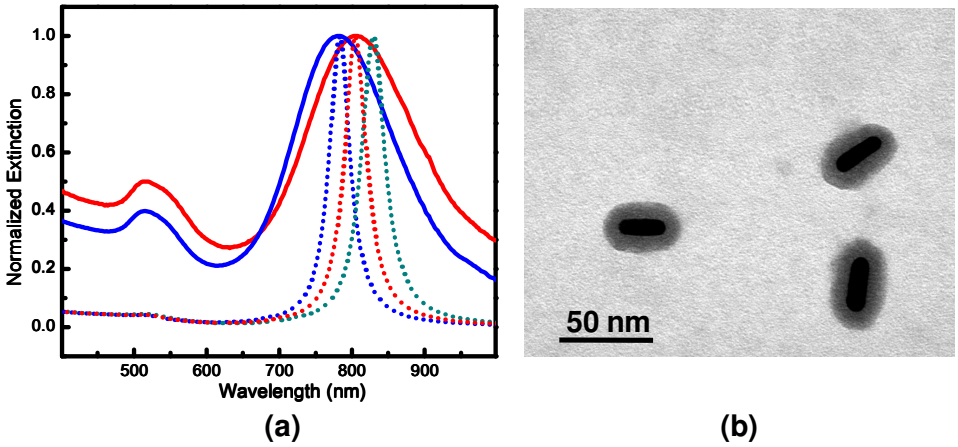

Fig. 2. (a) Experimental and simulated extinction spectra of the PEG-coated gold nanorods, and silica-coated gold nanorods, where solid blue (—) and solid red (—) curves correspond to experimental data of PEG-coated and silica-coated gold nanorods. The dotted blue (—), dotted red (—), and dotted green (—) curves correspond to FDTD calculated data of PEG-coated, porous silica-coated, and fused silica-coated gold nanorods, respectively. (b) TEM image illustrates one example of the silica-coated gold nanorods produced.

ratio and the very sensitive dependence of the peak position on the aspect ratio [4, 32]. The peak position of the simulation coincides with the experimentally determined position for a nanorod length of 34 nm and a diameter of 9 nm, which is very close to the experimental size and aspect ratio determined by TEM (Fig. 2(b)). The peak position of the simulated spectrum for the fused silica-coated nanorod is further to the red than seen in the experiment. While this could be due to a systematic reduction in aspect ratio during the coating process, we believe it is more likely due to a more porous nature of the silica synthesized by the modified Stöber method compared to the fused silica assumed in the simulation [26]. Reducing the refractive index from 1.459 for fused silica to 1.391 reproduces the peak position of the experiment, and this spectrum is also shown in Fig. 2(a). The calculated extinction cross sections agree well with the nanorod concentration estimated from the used gold ions in the synthesis and the measured extinction spectra.

The thermal stability of CTAB and PEG-coated gold nanorods, as well as silica-coated gold nanorods with 6 nm and 20 nm thickness was compared using UV-Vis spectroscopy. The longitudinal plasmon peak is a good indicator for shape changes of the nanorods, because the peak position strongly depends on the aspect ratio [5]. Indeed, after irradiating the aqueous

#124424 - $15.00 USD Received 18 Feb 2010; revised 29 Mar 2010; accepted 30 Mar 2010; published 13 Apr 2010

nanorod solutions with 300 laser pulses at various fluences, the longitudinal peak changes shape in all cases above some threshold fluence (Fig. 3). Fluences below 4 mJ/cm^2 did not induce any spectral changes of the longitudinal peak in all cases. However, fluences above 8 mJ/cm^2 induced a 10% amplitude decrease for the CTAB-coated gold nanorods, while no

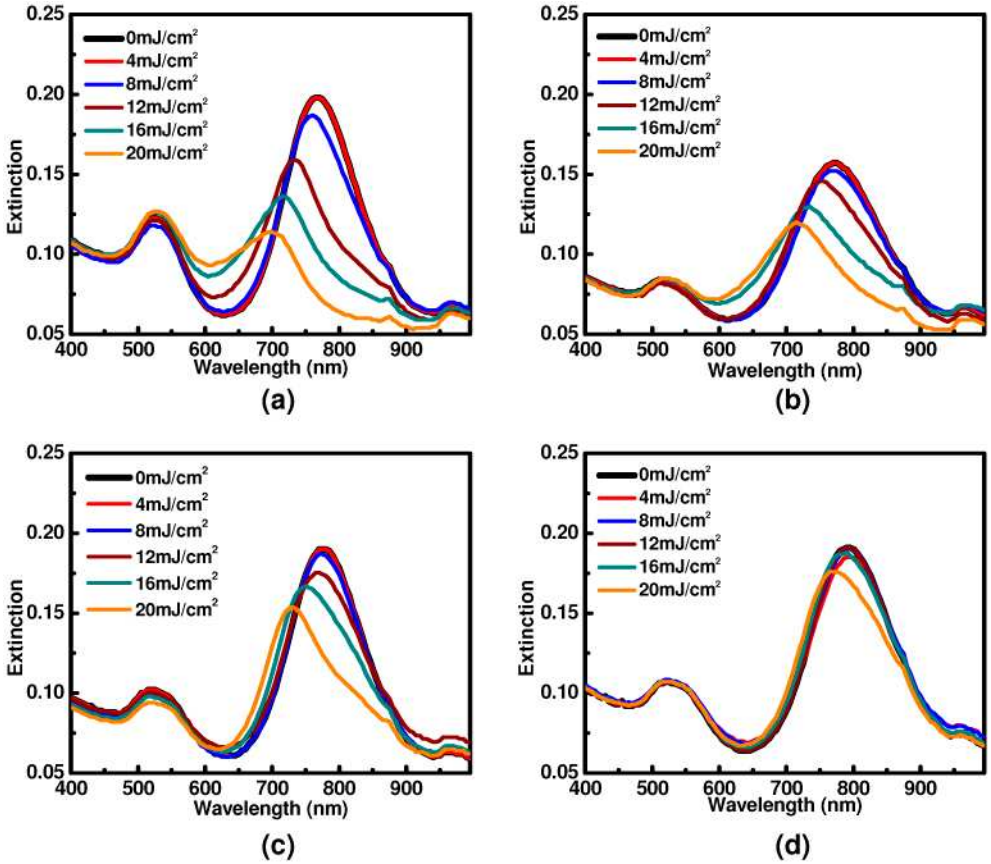

Fig. 3. Measured UV-Vis extinction spectra of (a) CTAB-coated gold nanorods, (b) PEGylated (PEG-coated) gold nanorods, (c) 6 nm silica-coated gold nanorods, and (d) 20 nm silica-coated gold nanorods before and after laser irradiation with various fluences.

changes were observed for the PEG-coated and silica-coated nanorods. Further increase of the fluence led to a dramatic decrease of the amplitude, a strong shift to the blue of the longitudinal peak, and a strong increase of the absorption in the 600–650 nm range, which all are consistent with a rounding of the gold nanorods. Bare PEG-coated nanorods showed the same spectral trends as CTAB-coated nanorods, only at slightly elevated fluences starting at 12 mJ/cm^2. In contrast, already a 6 nm silica shell induced a stabilizing effect, although above 12 mJ/cm^2 the peak also decreases and shifts to the blue at a similar rate as for the PEG-coated nanoparticles. However, no shoulder in the 600–650 nm range develops here, suggesting a different process of change and possible material loss. The 20 nm silica-coated gold nanorods, in contrast, are very robust and show no change in the spectrum under pulsed laser exposure, and only show a small spectral change of ~10% above 750 nm at 20 mJ/cm^2 (Fig. 3(d)). It is therefore clear that the uncoated gold nanorods change shape due to the nanosecond laser pulses, lowering their aspect ratio. Thick silica coating protects the gold nanorods, while thin silica coating shows only a limited protection, and material may be lost when the aspect ratio is reduced.

#124424 - $15.00 USD Received 18 Feb 2010; revised 29 Mar 2010; accepted 30 Mar 2010; published 13 Apr 2010

Figure 4 shows TEM images of PEG-coated and 6 nm and 20 nm silica-coated gold nanorods before and after 300 pulses of 7 ns duration and 20 mJ/cm^2 fluence each, whose corresponding UV-Vis spectra are shown as black and orange curves in Fig. 3(b), Fig. 3(c) and Fig. 3(d), respectively. PEG-coated gold nanorods changed from rod-shaped to either spherical, ellipsoidal, or "ϕ" shape – an ellipsoid with an equatorial thickening (Figs. 4(a-b)) first observed by Chang *et al.* [4]. In contrast, already a silica coating of around 6 nm improved the shape stability, and only few cases of severe shape change were observed (Figs. 4(c-d)). Instead, the pulsed laser irradiation caused a decrease in length and therefore aspect ratio of the gold cores from 3.9 ± 0.38 to 3.0 ± 0.25 (n=100). This can explain the blue shift of the plasmon peak in the spectrum (Fig. 3(c)). A further increase in the silica thickness to around 20 nm nearly completely stabilized the rod shape, and almost no shape deformation was observed after laser irradiation. Additionally, the heating of the gold core by the nanosecond pulsed laser irradiation did not cause any apparent morphological changes to the silica layer for either the 6 nm or the 20 nm thick shells.

FDTD simulations were performed to calculate extinction and absorption cross sections to confirm the interpretation of the experimental results, and the results are summarized in Fig. 5. Unprotected gold nanorods form ellipsoidal particles upon pulsed heating, which strongly shifts the resonance to the blue. In Fig. 5 spectra for ellipsoidal particles with circular

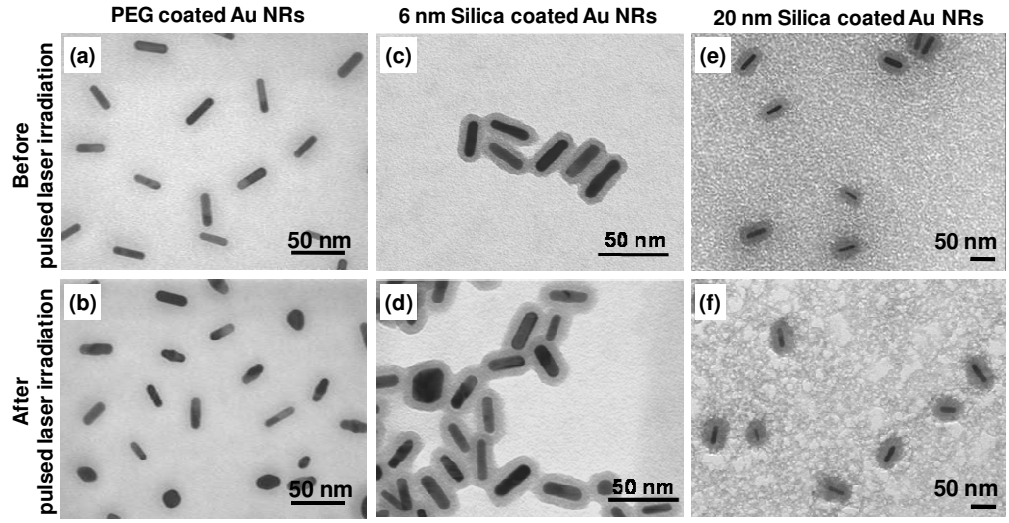

Fig. 4. TEM images show the morphology evolutions of various gold nanorods before and after 300 pulses of 20mJ/cm^2 laser irradiation. (a) and (b): PEG coated gold nanorods; (c) and (d): 6 nm silica-coated gold nanorods; (e) and (f): 20 nm silica-coated gold nanorods.

#124424 - $15.00 USD Received 18 Feb 2010; revised 29 Mar 2010; accepted 30 Mar 2010; published 13 Apr 2010

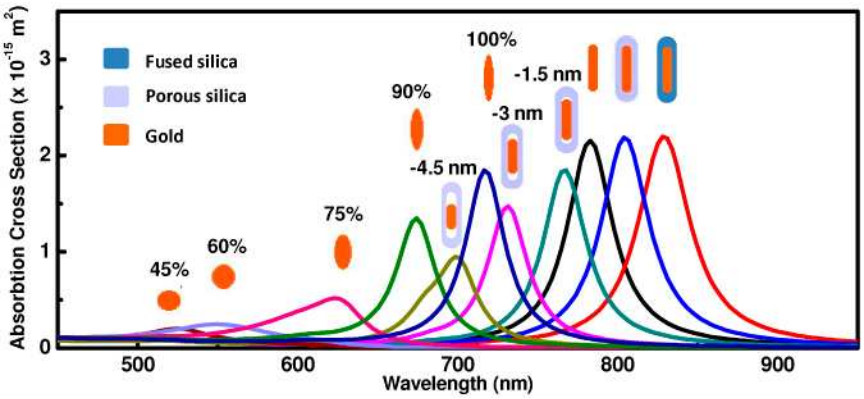

Fig. 5. FDTD simulated absorption cross section spectra for unpolarized light for various gold nanoparticles. Ellipsoids have the same volume as the original nanorod and are labeled as the fraction of the long axis relative to the original nanorod length. Shortened silica-coated nanorods are labeled for their reduction at each end. For details see the text.

cross section are shown that have the same volume as the original nanorod. The long axis is progressively shortened, and consequently the short axis progressively increased, going from a slightly rounded nanorod to a sphere. Spectra are labeled by the fraction of the long axis relative to the original nanorod length. Even pure rounding without changing the length (100%) already causes a strong shift to the blue. Further rounding with shortening of the long axis leads to resonances in the 600–650 nm range with strong shoulders to the blue (90% – 75%). Ultimately the spectrum of a sphere is reached (45%). Therefore already a small rounding effect leads to the increased absorption in the wavelength range of 600–650 nm seen for CTAB and PEG-coated gold nanorods. The reduction in elongation is accompanied by a strong reduction in absorption cross section that reproduces the trend in the experimental extinction spectra at higher fluences for the unprotected nanorods.

A closer examination of the TEM images of the 6 nm silica-coated gold nanorods shows a shrinking of the gold nanorod core in length due to the laser-pulse exposure, but the silica shell retained its shape, thus creating a small gap between the gold and silica at the tips of the rod (Fig. 6). The fractions of nanorods exhibiting this gap formation are outlined in yellow in Fig. 6(a). A similar hollow cap region between the gold nanorod and its silica coating is not found with the thicker silica coating. Simulations of such nanorods are shown in Fig. 5. Different from the simulation of the ellipsoids, only the long axis of the gold nanorods was shortened without changing the shape, while keeping the silica shell unchanged, and filling the void with water. Only very small reductions in nanorod length of 1.5, 3.0 and 4.5 nm at each end were simulated. These relatively small changes agree with the TEM images, and are sufficient to induce a blue shift of the resonance by about 50 nm and 100 nm, respectively. Shifts of this magnitude for such shortened nanorods in a silica shell confirm the spectra seen in Fig. 3. Most prominently, the resonances remain symmetric except for 4.5 nm reduction at each end, and the amplitudes do not decay as quickly; removing for instance 3 nm from each end corresponds to 18% length reduction and gives about twice the cross section compared to ellipsoids of similar length (Fig. 5). Also evident from the images is that the 6 nm silica-coated nanorods appear to form aggregates with fused silica shells, which is not found for either PEG-coated or 20 nm silica-coated nanorods. We assume this aggregation is induced by centrifugation, but additional investigation is required to completely define the cause.

The capability to produce a stable photoacoustic response is critical to photoacoustic image-guided photothermal therapy, since the photoacoustic contrast and the photoacoustic temperature mapping are based on the assumption that the absorbance of the photoabsorbers remains the same during imaging. The photoacoustic contrast depends on the difference in photoabsorber concentration and, at a constant concentration, the temperature induced

#124424 - $15.00 USD Received 18 Feb 2010; revised 29 Mar 2010; accepted 30 Mar 2010; published 13 Apr 2010

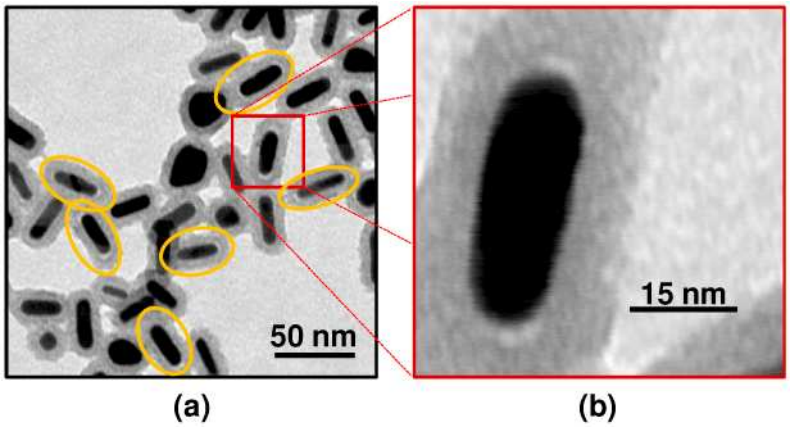

Fig. 6. (a) The TEM image illustrates the 6 nm silica-coated gold nanorods after irradiated by 300 pulses of 20 mJ/cm^2 laser light; the yellow circles indicate the nanorods which have hollow gaps between gold and silica. (b) The zoom-in view of the hollow gaps of a silica-coated gold nanorod. The image shows the gaps were formed in the tips and about 2 nm.

photoacoustic signal change is due to the change of the temperature dependent Grüeneisen coefficient. Clearly, a shape change due to the pulsed laser irradiation would cause false temperature measurements due to the change in absorption cross section. The stability of the photoacoustic response was investigated by measuring the photoacoustic amplitude generated by PEG-coated and 20 nm silica-coated gold nanorods during exposure to 300 pulses at fluences of 4 mJ/cm^2 and 18 mJ/cm^2 (Fig. 7). For both types of nanorods the photoacoustic amplitude was stable at 4 mJ/cm^2 as expected, because this fluence is below the damage threshold seen in the UV-Vis spectra (Fig. 3). At 18 mJ/cm^2, the signal from PEG-coated nanorods dropped by 40% in the first 100 pulses, while the 20 nm silica-coated gold nanorods produced a stable signal over the entire set of 300 pulses. It is important to notice that the experiment probes in all cases mainly the fraction of non-transformed particles, which remains constant for the 20 nm shell, but decreases for the PEG-coated nanorods. Therefore, gold-silica core-shell nanorods are a promising candidate for photothermal therapy, photoacoustic imaging using molecularly targeted nanoparticles.

Several mechanisms have been suggested for the increased stability seen with the silica-coated nanorods. The covalent binding of the PEG-thiol already leads to an increased stability, indicating its role in the stabilization of surface gold atoms or a change in the interfacial heat resistance; the influence of the chemical nature of the environment close to the nanorod surface has been shown by Mohamed *et al.* [33]. PEG induced stability also agrees with the increased thermal stability of PVA stabilized nanorods [17]. Another factor could be the steric barrier created by a rigid encapsulation, as has been shown for carbon and PMMA [21]. Especially the fact that PMMA only stabilized the rods significantly below the glass transition would speak for such a mechanism, as would our result that shows an undeformed silica shell with a shortened gold core. Silica stabilization of gold nanorods has also been demonstrated under annealing up to 200 °C, which also showed a small change in the structure of the silica as judged by the longitudinal plasmon peak position [25]. The slight red shift seen in these silica-coated nanorods synthesized using the layer-by-layer technique, is not found in our experiments. This difference may be due to our gold-silica coupling agent – we use PEG thiol that is chemically bound to both the gold and the silica, which could influence the silica structure. Alternatively, the longer time-scale of the heating could lead to less stress in the silica in our experiments. Finally, a change in the thermal conductivity could lead to an improved cooling due to a more efficient heat transfer. The influence of the heat transfer to the environment on the stability of nanorods has been shown for femtosecond laser pulses [17,34]. Silica has a significantly higher thermal diffusivity compared to water and the

#124424 - $15.00 USD Received 18 Feb 2010; revised 29 Mar 2010; accepted 30 Mar 2010; published 13 Apr 2010

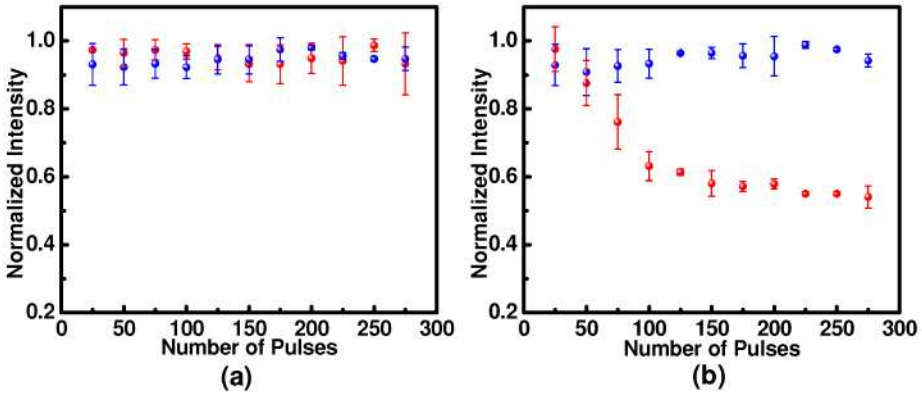

Fig. 7. Photoacoustic signal intensity of PEG-coated gold nanorods (red scatters) and silica-coated gold nanorods (blue scatters) versus number of pulses with fluence (a) 4 mJ/cm^2 and (b) 18 mJ/cm^2.

thickness-dependent thermal stability enhancement we have found could be in part due to the faster heat distribution over a larger area. However, the thermal relaxation time which is defined as d^2/α, with α the thermal diffusivity, is still shorter than the pulse width of the laser even for a thickness of d = 20 nm for both water and silica. In addition, the more porous structure of silica fabricated by the Stöber method is not considered, which has been shown to play an important role [34]. The reduction in nanorod length at high laser irradiation for thin silica shells may suggest that gold nanorods may shed atoms, an effect seen with silver but not with gold [21]. For photothermal therapy we expect the temperature increases achieved by continuous heating to be lower than the peak temperatures in transient temperature pulses used in this study. Increased stability during continuous heating due to a coating layer has been shown [17,21].

Furthermore, we have observed that under the same experimental conditions the silica-coated gold nanorods generate significantly higher photoacoustic signal compared to the PEG-coated gold nanorods [27]. The difference of the photoacoustic signal amplitude could be attributed to several factors including the differences in heat conductivity and Grüeneisen parameter of water and silica, field confinement due to the higher refractive index of silica compared to water, or other factors that increase the gold-silica core-shell nanorods efficiency in photon-heat and heat-pressure conversion. The detailed analysis of this phenomenon, however, is outside of the scope of the current paper.

7. Conclusion

In this study gold-silica core-shell nanorods with controllable silica thickness were produced. Their stability in aqueous solution to nanosecond high-energy laser pulses at the surface plasmon resonance was analyzed using UV-Vis spectroscopy, electron microscopy, and FDTD numerical simulation. Silica-coated gold nanorods retain the superior optical properties of bare gold nanorods, and they are thermally more stable under high-energy nanosecond laser irradiation compared to PEG-coated gold nanorods. Finally, the effectiveness of gold-silica core shell nanorods as a stable photoacoustic contrast agent was demonstrated. The results of our study suggest that gold-silica core-shell nanorods are a promising candidate for molecular photoacoustic imaging and image-guided molecular photothermal therapy.

Acknowledgments

Partial support from National Institutes of Health under grants CA149740, CA141203, EB008101 and CA135315 is acknowledged.

#124424 - $15.00 USD Received 18 Feb 2010; revised 29 Mar 2010; accepted 30 Mar 2010; published 13 Apr 2010

#124424 - $15.00 USD Received 18 Feb 2010; revised 29 Mar 2010; accepted 30 Mar 2010; published 13 Apr 2010